JOURNAL OF MATERIALS SCIENCE 7 (1972) 367–387

The Fracture Behaviour of Polyethylene Terephthalate

J. S. FOOT, I. M. WARD
Department of Physics, University of Leeds, UK

Tensile, notched tensile and cleavage tests have been carried out on amorphous and crystalline polyethylene terephthalate of different molecular weights.

At − 160°C where the materials are brittle, the brittle strengths of the amorphous materials are slightly molecular-weight-dependent at high and medium molecular weights: the high molecular weight leads to higher strength than the medium. However, the low-molecular-weight material has a very much lower brittle strength. Surface studies suggest that this sudden change is the change from failure from crazes in the high- and medium-molecular-weight material to failure from inherent flaws in the low-molecular-weight material. The crystalline material is weaker than the amorphous, failure arising from inherent flaws in every instance.

It was found that the notched tensile and cleavage results represent crack propagation from very blunt cracks with large surface energies. The cleavage results indicate very little difference in the materials at − 160°C but substantial differences at + 20°C. Crystalline samples have generally consistently higher fracture surface energies than the amorphous The low-temperature results substantiate the role of flaws and crazes indicated in the tensile tests. The 20°C results have been interpreted using tensile data to evaluate the work done to failure at a blunt crack tip.

1. Introduction

A recent paper [1] describes the examination of the tensile behaviour of polyethylene terephthalate over a wide range of temperatures. Particular attention was paid to obtaining a general impression of the effects of molecular weight and crystallinity on the type of failure observed, and specifically whether this was of a ductile or brittle nature. Both unnotched and notched specimens were subjected to tensile tests over the temperature range − 200 to + 100°C. At low temperatures all specimens failed in a brittle manner and the brittle strength fell with decreasing molecular weight. There was also a clear fall in brittle strength with crystallisation. In the present paper this preliminary work has been extended by making more extensive tensile tests and by undertaking further notched tensile tests and cleavage tests.

2. Experimental

2.1. Uniaxial Tensile Tests

2.1.1. Preparation of specimens

Specimens for tensile tests were prepared by injection moulding, different conditions being chosen for the different grades of polymer to ensure that no crystallisation occurred at this stage. The dimensions of the specimens are shown in fig. 1a. To remove residual orientation the specimens were annealed at 70°C for 12 h. The density of the specimens after annealing was found to be 1.337 ± 0.002 g cm^{-3}. This compares with a reported value of 1.335 g cm^{-3} for amorphous PET, and shows that negligible crystallinity is introduced.

Crystalline specimens were prepared by heat crystallisation at 170°C for 30 min. This produced specimens of density 1.378 ± 0.002 g cm^{-3}, which on the simplest estimate correspond to a crystallinity of 36%, assuming a density for the crystal unit cell of 1.455 g cm^{-3}.

2.1.2. Tensile measurements

The tensile measurements were carried out on an Instron tensile testing machine and the specimens were mounted in the jig shown in fig. 1b. This arrangement enabled low temperatures to be attained by immersing the jig in a liquid nitrogen

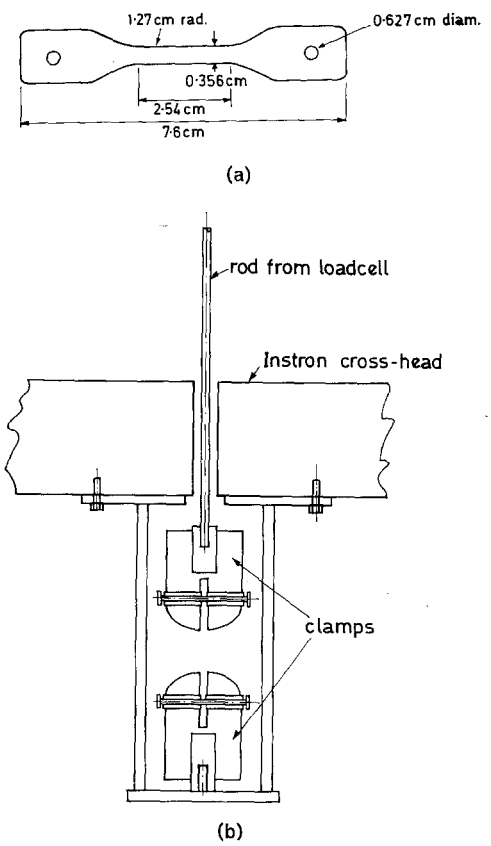

Figure 1 (a) Dimensions of dumbell samples. (b) Jig for pulling sample beneath cross-head.

dewar. A preliminary experiment performed on dumbell specimens cut from isotropic PET sheet of thickness 0.02 cm, showed that when the samples were in contact with liquid nitrogen they crazed and failed at comparatively low stresses and large strains of the order of 15%. By protecting the sample from the coolant by a thin copper can, temperatures of the order $-160 \pm 10°C$ were obtained and the load extension curves were those for a typical brittle material. The samples still crazed but these crazes were few and mainly healed when the sample was warmed at 20°C. Although the effect was not so marked on thick injection-moulded samples the tests were still carried out protected from the coolant and at a temperature of $-160° \pm 10°C$. The copper can also enables the samples to cool slowly rather than subjecting them to thermal shock.

The temperature was monitored with a thermocouple held near to the sample. A constant strain rate of 4.5×10^{-2} sec^{-1} was used.

2.2. Notched Tensile Tests

2.2.1. Preparation of specimens

Two types of specimens were used for the notched tensile tests; thick specimens prepared from injection-moulded plaques 0.195 cm thick and thin specimens cut from sheet of thickness 0.02 cm. The thick specimens were annealed at 70°C for 12 h to remove any residual orientation and the birefringence of the sheet was found to be less than 5×10^{-5}, indicating that there is a negligible degree of molecular orientation. The molecular weight of the injection-moulded samples was in the range $\bar{M}_n$ 12000 to 30000. The molecular weight of the sheet sample was $\bar{M}_n = 16000$.

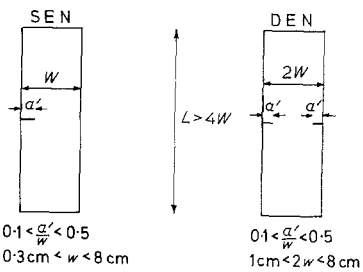

Figure 2 Geometry of a typical singly edged notched and doubly edged notched specimen (termed **SEN** and **DEN** respectively).

A typical geometry of a singly and doubly notched specimen is shown in fig. 2. The length of the specimen not in the clamps was greater than double its width. The injection-moulded samples were tested with widths from 0.3 to 3.5 cm and sheet samples with widths from 0.5 to 8 cm.

The injection-moulded samples were notched by first putting a saw blade into the edge and then pushing a razor blade in from this. The length of two notches of a doubly notched specimen could be made very nearly equal. The sheet samples were notched by cutting with a razor blade.

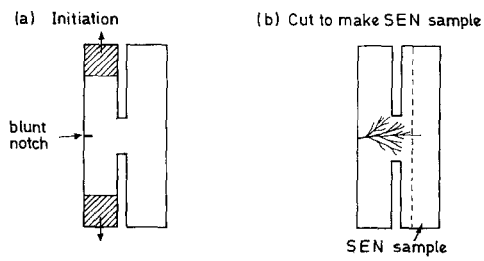

Figure 3 Schematic diagram of the formation of fine notches in sheet material.

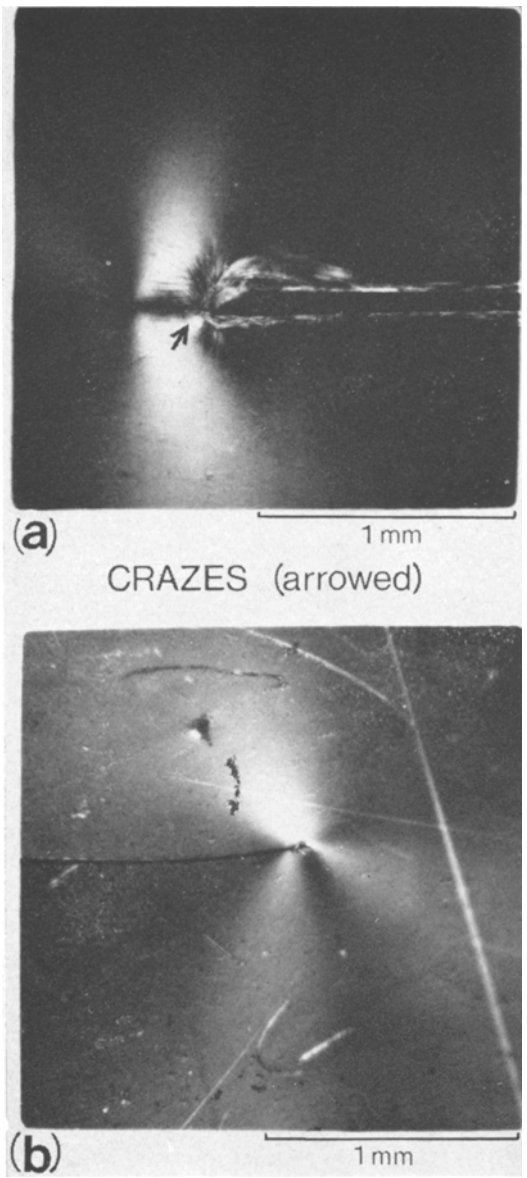

Figure 4 Notches in sheet material.

A novel method was developed to generate a very fine notch in the sheet samples. This involved cutting a specimen to the shape shown in fig. 3a. These specimens were then extended at $-40°C$ at 0.2 cm min^{-1} in the tensometer. In a number of cases the subsequent crack bifurcated in such a manner that a single fast crack travelled into the region of the specimen enclosed by the dotted line in fig. 3b. A new test specimen could then be produced by cutting out this region.

Figs. 4a and b are optical micrographs of the notches produced by a razor blade and by this novel method, respectively, viewed with the polariser and analyser crossed. This shows very much less plastically deformed region associated with the latter notch than the former one.

The notch depth a to the width of the doubly notched specimen W or $W/2$ for the singly notched specimen was varied between the limits [2]

$$0.1 < a/W < 0.5$$

2.2.2. Test procedure

Notched tensile tests on the specimens were undertaken at -100, -50, and $+20°C$, at a constant cross-head speed of 0.007 cm sec^{-1}. The temperature was measured with a thermocouple, -50 and $20°C$ being attained in an Instron cabinet, and $-100°C$ in a copper jacket through which cold nitrogen was passed.

Linear elastic fracture mechanics was used to determine the *stress intensity factor* K, and the *fracture toughness* was taken to be K_c, the critical value of this quantity at failure. K_c was determined for these materials under conditions in which

(a) the material behaved in a brittle manner, i.e. the load extension curves are linear up to fracture or there is no gross yielding of the material, and (b) the material broke from the notches, i.e. the imposed notches were more severe than the natural flaws.

The formula used to compute K_c [3] is

$$K_c = \sigma \sqrt{W \tan\left(\frac{\pi a}{W}\right) \pm 0.1 W \sin\left(\frac{2\pi a}{W}\right)} \quad (2.1)$$

where σ is the failure stress calculated on the cross-sectional area, W is the width of the doubly notched specimen and twice the width of the singly notched specimens and a the depth of the notch.

The nature of failure of both the thick and thin specimens is typified by the optical micrographs in fig. 5. Fig. 5a shows the fracture surface and fig. 5b the side view of the broken pieces. This shows slow growth from the notch; fig. 5a, which has a very smooth surface and a rough surface which starts at the point of bifurcation, fig. 5b. Thus it has been possible to define K_c' and K_c'' which are the values of K_c for cracks of length a' and a'' where a' is the original notch depth and a'' is a' plus the length of the slow crack growth. These distances were measured with a travelling microscope, limited accuracy being obtained due to the curved crack front.

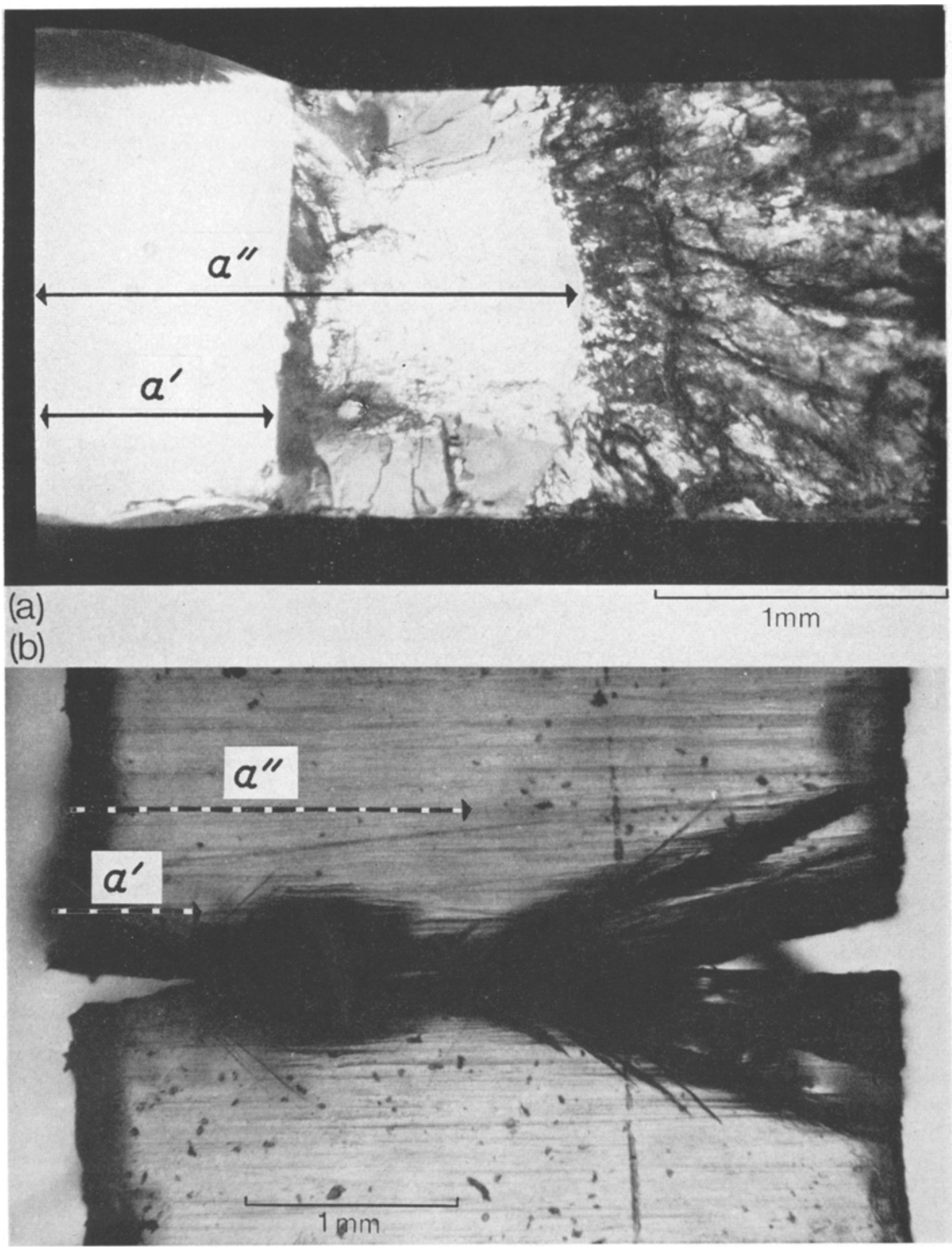

Figure 5 A tested notched tensile specimen.

2.3. Cleavage Tests

2.3.1. Preparation of specimens

The specimens for cleavage tests were cut from injection-moulded discs prepared by identical procedures to those described for the tensile test specimens in section 2.1.1 above. Similar procedures were followed to prepare amorphous specimens and crystalline specimens. In this case the amorphous specimens were annealed at 70° C for 12 h both before and after the machining of the actual cleavage specimens and the crystalline specimens were crystallised by heating at 170°C for 30 min before machining, and annealed for 12 h at 120°C, after machining.

The specimen geometry was determined by three main considerations.

(1) Because amorphous specimens were required, the thickness of the specimens must be small enough to allow rapid quenching in the mould. In this way crystallisation in the mould is reduced to a negligible amount.

(2) For simplicity of analysis, the crack should be in a purely opening mode. This restricts the length of the crack compared with the other dimensions if the arms of the cleavage specimens are not to buckle.

(3) Again for simplicity of subsequent analysis, a wedge opening loaded specimen (WOL) of the type designed by Manjoine [4] is desirable. Such specimens are designed to have a stress intensity factor independent of crack length. This has three advantages. First, calibration is more accurate because the compliance of the specimen is linearly dependent on crack length, and is not determined from the gradients of a curve. Secondly, once the specimen compliance is obtained the position of the crack need not be accurately known. This is desirable for opaque crystalline specimens and for working at low temperatures where it is difficult to monitor the crack front visually. Finally, the crack speed is proportional to the speed at which the beams are opened, and can therefore be simply controlled and calculated.

The cleavage specimens were cut from injection-moulded discs of 11.5 cm diameter and 0.345 cm thickness. The specimen geometry is shown in fig. 6a, the exact shape being chosen from computed values of the stress intensity factor evaluated for WOL specimens by Srawley and Gross [5].

Loading was by pins passing through lobes on the wings of the specimen. It is considered that these lobes do not affect the analysis, as for small openings only the line of action of the load is important.

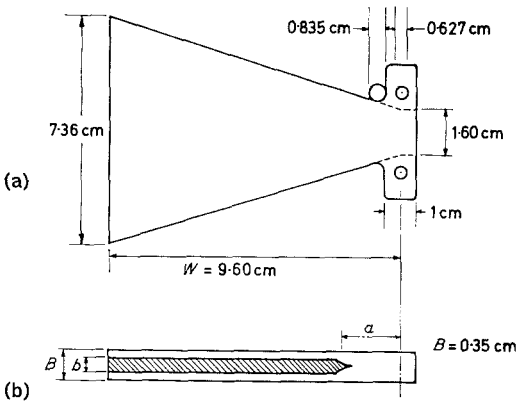

Figure 6 (a) Geometry of cleavage specimens. (b) Swallow tail cut.

It is necessary to constrain the crack growth to the central line of the specimen by cutting grooves. This technique is common in cleavage work, and has previously been used by Berry [6], Broutman and McGarry [7] and others. In this case the grooves were cut with a milling blade of thickness 0.015 cm to an equal depth on both sides of the specimen. The ratio of the remaining crack width b to the width B of the specimen was varied from $\frac{1}{6}$ to $\frac{1}{2}$ without producing any detectable difference in the results obtained. The initial crack tip was cut with a saw blade to give the swallow-tail shape [7] shown in fig. 6b.

2.3.2. Test procedure

The cleavage specimens were mounted in the assembly shown in fig. 1b, so that the tensile load could be applied by the Instron tensile testing machine. Tests were carried out at $20 \pm 2°C$ and $-160° \pm 10°C$. The temperatures were measured by a thermocouple, the low temperature being attained by immersing the assembly in liquid nitrogen. The specimen was again protected from the coolant by a copper can.

Because the assembly was designed to minimise thermal conduction it is not very stiff. However, its compliance was measured to be 1.5×10^{-10} cm dyne^{-1}, which is small compared with that of the polymer cleavage specimens used here.

Tests were carried out with cross-head speeds in the range 0.0001 to 0.02 cm sec^{-1}. The initial compliance was recorded against the initial crack length. The load at which the crack moved was then recorded, and showed fluctuations of

$\pm$ 5%. The sample was unloaded after growing the crack for a distance between 1 mm to 4 cm, the new crack position noted, and the test carried out again until the crack length was 6 cm, at which point the stress intensity factor becomes a function of crack length.

The width of the crack at 1 cm intervals was measured with a travelling microscope after complete cleavage of the sample.

The fracture surfaces were studied with an optical microscope using both transmitted and incident light and in a scanning electron microscope.

3. Results and Discussion

3.1. Uniaxial Tensile Tests

Tensile tests were undertaken at $-$ 160°C on four grades of polymer corresponding to four values of number average-molecular-weight $\bar{M}_n$. For a condensation polymer this defines the molecular weight uniquely. In each case ten specimens of amorphous and heat crystallised polymer were tested. The results are shown in fig. 7, where the mean failure stress and one standard deviation about that mean is shown.

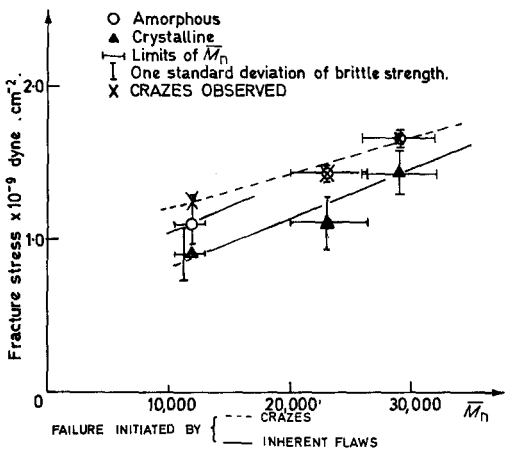

Figure 7 Brittle strength of amorphous and crystalline PET at $-$ 160° C and strain rate of 6×10^{-3} sec^{-1}.

Several features of the fracture behaviour are apparent from these results. First, the mean values of the brittle strength fall with decreasing molecular weight for both amorphous and crystalline material. In the amorphous material this fall is not uniform, but as reported previously [1], there appears to be a threshold below which much lower strengths are observed. Secondly, the strengths of the crystallised polymer are always less than those of the corresponding amorphous polymer. Finally, the standard deviations observed for the crystalline polymers and for the low-molecular-weight amorphous polymers are much greater than those observed for the medium- and high-molecular-weight amorphous polymers.

These features considered together suggest that there may be a difference between the fracture mechanisms in the medium- or high-molecular-weight amorphous polymers and the other polymers tested. This was confirmed by examination of the fracture surfaces using optical microscopy and a scanning electron microscope. It appears that the medium- and high-molecular-weight amorphous polymers failed from crazes, whereas the other polymers failed from internal flaws. Fig. 8b shows an optical micrograph of the surface of a high-molecular-weight specimen (viewed in reflected light). The smooth outside parts of the surface are associated with the craze and the rough central part with fast crack growth. The crazes in the medium- and high-molecular-weight material could also be observed in an optical microscope by reflection of light in the bulk of the material, fig. 8a, and these crazes show a tendency to heal up when the specimens are warmed to room temperature.

The low-molecular-weight amorphous specimens, with the exception of those results marked by a cross in fig. 7, failed at internal flaws. The crosses represent failure from crazes. Fig. 9 shows an optical micrograph of failure from a central flaw in a low-molecular weight amorphous specimen. This surface shows a smooth mirror zone and a rough section growing from this.

The differences in the magnitude of the standard deviations are also consistent with a change in mechanism between the medium- or high-molecular-weight amorphous specimens and all the other specimens. It is suggested that the growth of crazes is a more reproducible process and associated with a more consistent property of the bulk of the material. Little work has been carried out on the actual size of crazes but the work of Kambour [8] for polycarbonate suggests that crazing behaviour is fairly reproducible (see also reference [9]).

It was therefore concluded that all the crystalline specimens and the low-molecular-weight amorphous specimen fail from inherent flaws, but that in the higher-molecular-weight amorphous specimens failure initiates from a craze. The low-molecular-weight amorphous

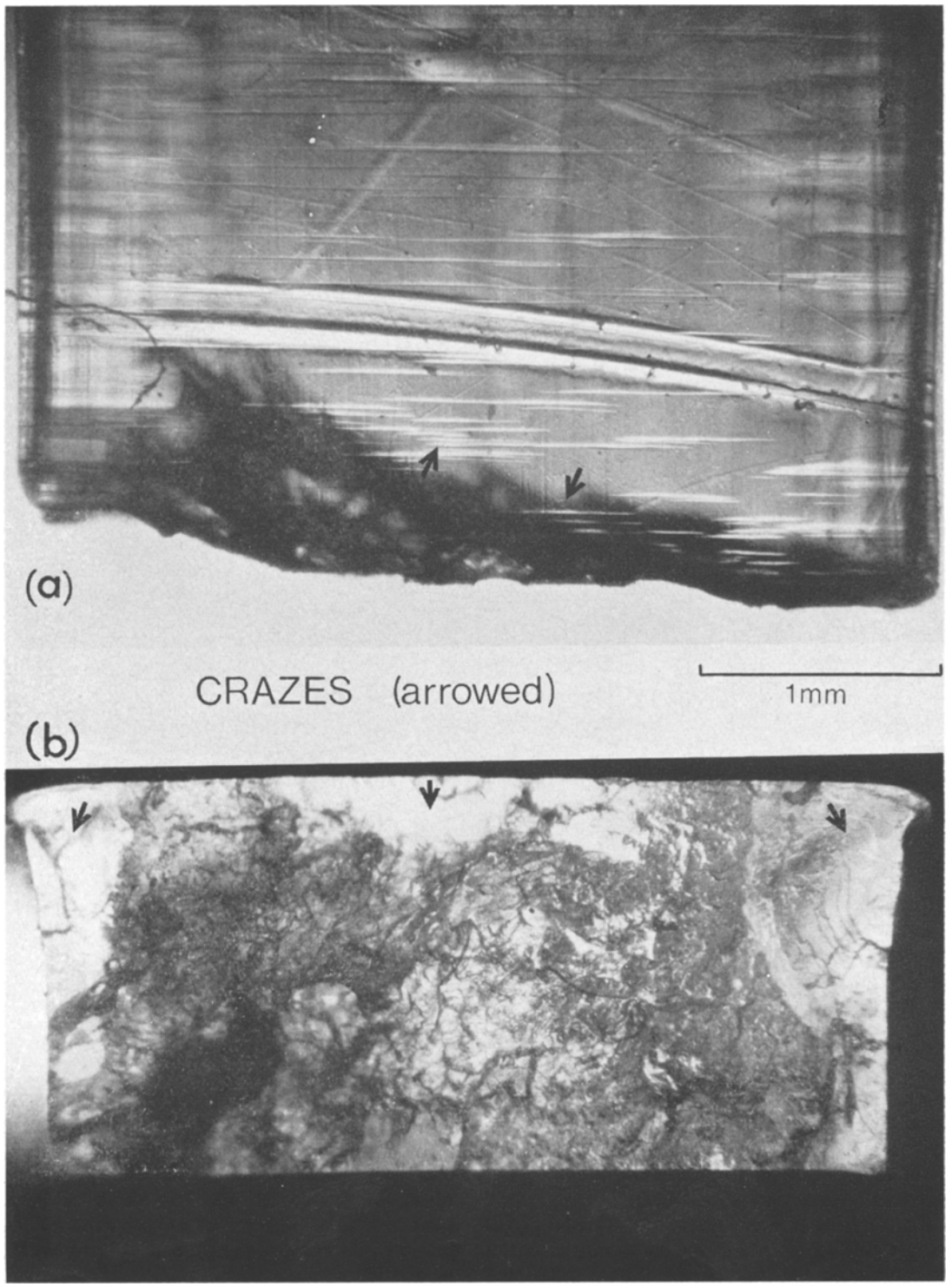

Figure 8 Tensile failure from crazes at – 160° C.

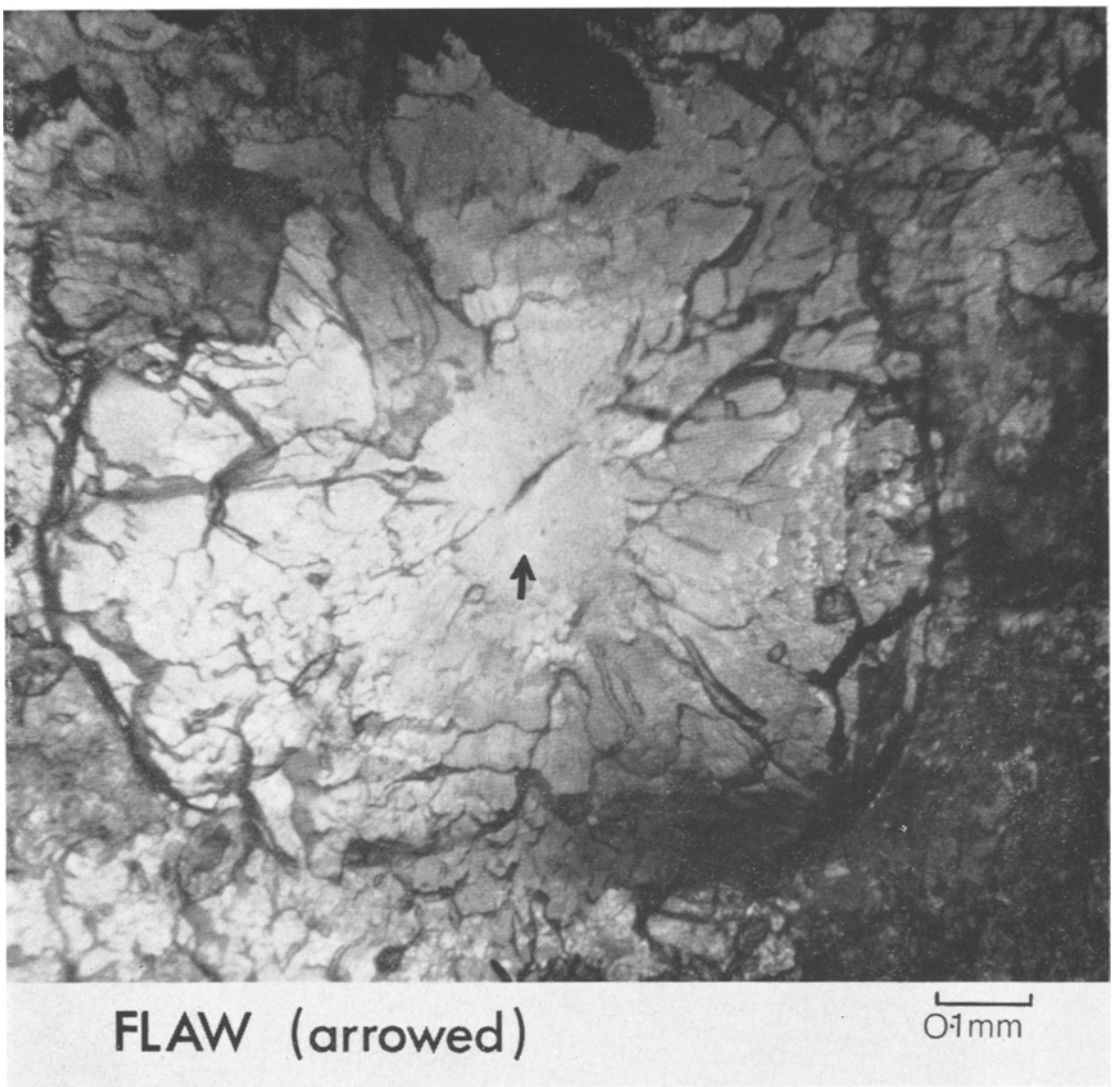

Figure 9 Tensile failure from an inherent flaw at − 160° C.

polymer does not generally reach the necessary stress for crazing to occur, because a flow can cause premature failure. The crystalline specimens all fail from flaws at lower stresses than their amorphous counterpart, but as in the case of the amorphous polymer, the brittle strength is still molecular-weight-dependent.

An estimate of the fracture surface energy for samples failing from internal flaws was obtained by measuring the size of the mirror zone and using this as the flaw size. The surface energy was calculated using the Griffith expression for an infinite medium,

$$\gamma_p = \frac{\sigma_B^2 \, a \, \pi}{2E} (1 - \nu^2) \qquad (3.1)$$

where γ_p is surface energy, σ_B the brittle stress, E the Young's Modulus and ν Poisson's ratio. It was only possible to obtain an approximate value for a (see fig. 9). The value of γ_p for amorphous low-molecular-weight material was found to be approximately 5×10^5 erg cm^{-2} at − 160° C.

The depth to which crazes have to grow to cause failure is larger than the size of the mirror zone around a flaw. This suggests that the

surface energy of failure from crazes of the high medium-molecular-weight amorphous materials is higher than 5×10^5 erg cm^{-2}. A more exact value is difficult to obtain for these materials because the crazes are of comparable size to the dimensions of the specimen and therefore the approximation of an infinite medium used in equation 3.1 will not hold.

3.2. Notched Tensile Results

Notched tensile tests were, on the whole, difficult to perform because of the restrictions discussed in section 2.2.2. The results on the sheet material proved to be more successful and easier to interpret. These results are discussed in section 3.2.1. The results for injection-moulded samples, where molecular weight could be varied, are discussed in section 3.2.2.

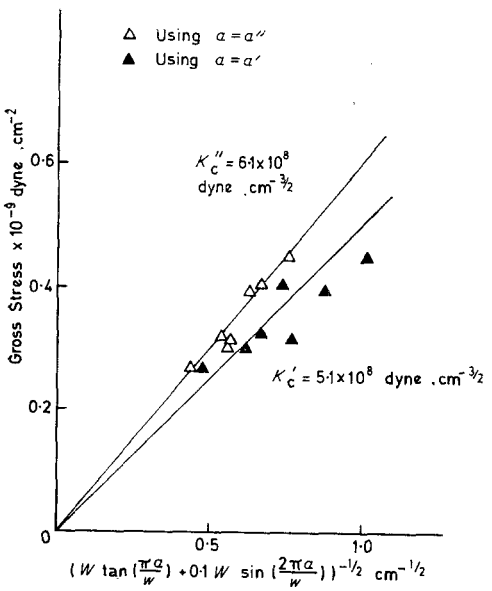

Figure 10 Values of K_c' and K_c'' found from SEN and DEN crystalline sheet material at 20° C.

3.2.1. Notched tensile results on sheet of thickness 0.02 cm

Fig. 10 shows the gross cross-sectional stress as a function of the reciprocal of the square root of the crack length (modified by the finite width of the samples) for heat crystallised sheet measured at 20°C. The original crack depth a' and the notch depth plus the slow crack growth region a'' are shown. This gives values of $K_c' = 5.1 \pm 0.2 \times 10^8$ dyn $cm^{-3/2}$ and $K_c'' = 6.1 \pm 0.1 \times 10^8$ dyn $cm^{-3/2}$. The amorphous sheet material is not brittle at room temperature but draws in the reduced cross-sectional area. Table I shows the mean value of K_c' and K_c'' and one standard error about the mean for about eight samples of amorphous and crystalline sheet each tested at 20, − 50, and − 100°C.

As expected, K_c'' at 20°C is more reproducible than K_c'. This is because at the maximum failure stress the crack length is closer to a'' than a'. At lower temperatures the difference betewen K_c'' and K_c' is not important because there is little slow crack growth. As a result of this the observed standard error in K_c'' or K_c' is larger as it is more dependent on the original notch root radius. The values of K_c'' and K_c' fall with decreasing temperature in the range observed. The crystalline material although notch brittle at higher temperature is in fact tougher when compared with the amorphous material. This is consistent with its higher yield strength [1]. The results using the sharper notches produced by a fast bifurcating crack described in section 2.2.2 gave identical results to those of table I at all temperatures. This shows that even though the notches produced by this method have a smaller notch root radius than those made from a razor blade they behave in the same manner. This means the cracks are blunting themselves. It is interesting that a fast crack when brought to a halt in a material is then as blunt as a razor notch. In fact examination of these cracks does show some bifurcation at the end, and crazes form when they are reopened.

TABLE I Values of K_c' and K_c'' for amorphous and crystalline sheet.

	K_c' or K_c'' in dyn/cm$^{3/2}$	Temperature		
		20°C	− 50°C	− 100°C
Amorphous	K_c'	Not notch	$5.0 \pm 0.4 \times 10^8$	$3.5 \pm 0.3 \times 10^8$
	K_c''	brittle	$5.0 \pm 0.4 \times 10^8$	$3.5 \pm 0.3 \times 10^8$
Crystalline	K_c'	$5.1 \pm 0.2 \times 10^8$	$4.6 \pm 0.3 \times 10^8$	$3.7 \pm 0.3 \times 10^8$
	K_c''	$6.1 \pm 0.1 \times 10^8$	$5.3 \pm 0.3 \times 10^8$	$3.8 \pm 8.3 \times 10^8$

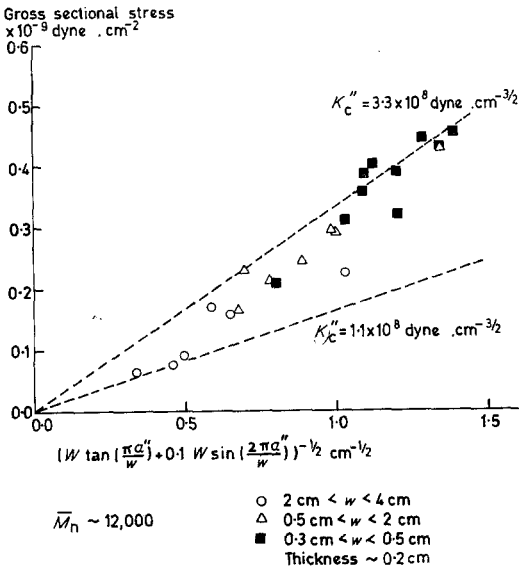

Figure 11 Variation of K_c'' from SEN measurements with specimen geometry for amorphous low-molecular-weight material at 20° C.

In translating the value of K_c into surface energy γ_p it is necessary to define the state of stress [10]. If plane strain exists at the crack tip then:

$$K_c^2 = 2E\gamma_p(1 - \nu^2) \tag{3.2}$$

and if plane stress exists then:

$$K_c^2 = 2E\gamma_p \tag{3.3}$$

where E is the Young's Modulus and ν the Poisson's ratio.

There is a plastically deformed region of size r_p around the crack tip. On a simple basis [10] r_p is calculated as the region in which the stresses are sufficient to cause yield assuming that the region does not affect the stress analysis.

$$r_p = \frac{K_c^2}{2\pi\,\sigma_y^2} \tag{3.4}$$

where σ_y is the yield stress. Thus at 20° C where K_c'' is 6.1×10^8 dyn cm$^{-3/2}$, r_p is of the order 0.2 cm assuming a yield stress of the order 6×10^8 dyn cm^{-2} [1].

Thus r_p is greater than the thickness of the sheet and therefore a state of plane stress exists [2]. The surface energy for plane stress failure at 20° C is therefore 7.5×10^6 erg cm^{-2}, using a value of $E = 2.4 \times 10^{10}$ dyn cm^{-2} [14]. The value of plane stress energies are always larger than those of plane strain because flow is reduced in the latter case.

3.2.2. Notched tensile results on injection-moulded samples of thickness 0.195 cm

At 20° C the medium- and high-molecular-weight amorphous material drew from the notches and therefore the tests could not be performed on these materials. At − 100° C, however, brittle failure of all the materials resulted but not from the imposed notches. Failure initiated from a flaw and spread to the notches. Thus no value of K_c could be obtained. Attempts to insert sharper notches by cooling the material in liquid nitrogen and then insertng the razor blade did not succeed in providing sharp enough notches.

Notched tensile results were therefore only obtained on the low-molecular-weight amorphous material and the medium-molecular-weight crystalline material at + 20° C. Fig. 11 is a plot of gross cross-sectional stress versus the reciprocal of the square root of crack length (modified by the finite width W) for low-molecular-weight amorphous material at 20° C. The crack length is taken as a'' rather than a' as this has been shown above to be a better approximation of its value at failure. The results do not give a linear relationship passing through the origin.

$K_c'' = 3.3 \times 10^8$ dyn cm$^{-3/2}$ for $a'' \simeq 0.1$ cm

and

$K_c'' = 1.1 \times 10^8$ dyn cm$^{-3/2}$ for $a'' \simeq 2$ cm

Likewise K_c' is not a constant. One possible correction would involve the addition of an amount r_p to the crack length, where r_p is the size of the plastic zone defined previously. This does not explain the result because the shorter notch depth would give a larger increment in the critical stress intensity factor. A more acceptable explanation is that r_p (which using relationship 3.4 is 0.05 cm for $K_c'' = 3.3 \times 10^8$ dyn cm$^{-3/2}$) is comparable with the thickness of 0.198 cm. The state of stress for the small a'' is therefore nearer to plane stress than for the larger a''. Thus K_c'' falls with increasing crack length.

The same behaviour was observed with the medium-molecular-weight crystalline samples at 20° C. Here K_c'' varies from 4.5 to 5.9×10^8 dyn cm$^{-3/2}$ for long and short crack lengths respectively.

The curved nature of the mirror zone as shown in fig. 5a is furher evidence that the state of stress in these specimens is transitory between plane strain and plane stress.

3.2.3. Bifurcation

As observed previously in the notched tensile tests, both thick and thin specimens failed ultimately by bifurcation. Bifurcation in isotropic materials is believed to arise when the crack reaches a speed comparable to the speed of the elastic waves [11]. Two points are of interest. Firstly, that not all the bifurcated cracks are joined up. It is possible for a secondary crack to start near but not from the original crack. Presumably this initiates in the rapidly changing stress field at a flaw. Secondly, a fast bifurcating crack when it slows down has a very smooth surface which exhibits interference colours [19]. The mirror zone at the initiation of fracture, although as smooth, does not show colours. This indicates that a crack which is slowing down has a reoriented layer of the order of a few wavelengths of light, whereas the mirror zone has a larger reoriented layer. This provides further understanding of the large surface energies ($\sim 10^6$ erg cm^{-2}) observed in initiation of fracture from notches, compared with those obtained in the uncontrolled fast fracture of unnotched specimens which are $\sim 10^5$ erg cm^{-2}.

3.3. Cleavage Results

3.3.1. Surface energy data

As explained in section 2.3.1 the sample geometry was chosen to have a stress-intensity factor K which is almost independent of crack length. The value of K for various values of a/W is shown in table II in terms of a dimensionless quantity $KBW^{\frac{1}{2}}/P$. B and W are the constant dimensions defined in fig. 6, and P is the load. These results due to Gross and Srawley [5], show that there is only a small variation in K/P as a changes from 2 to 6 cm.

The results have been calculated on the basis of surface energy rather than the critical stress intensity factor K_c to eliminate assumptions regarding linear elasticity and plane strain. They can, however, be compared with the critical stress intensity factor using the plane strain relationship (3.2.)

Referring to fig. 12, the work done in increasing the crack length by Δa is $\frac{1}{2}P^2\,\Delta C$ so that the surface energy is given by

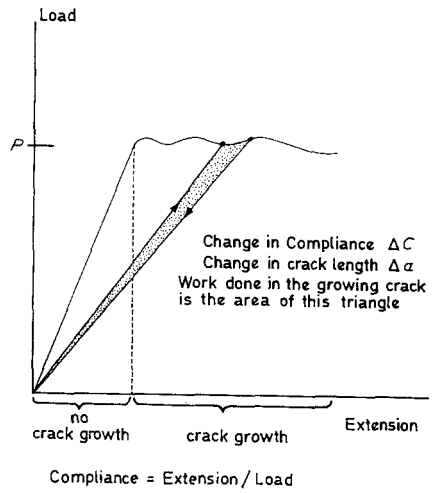

Figure 12 Schematic load/extension curve of cleavage sample.

$$\gamma_p = \frac{P^2}{4b}\frac{dC}{da} \tag{3.5}$$

where C is the compliance and b the width of the crack; this is the Irwin-Kies relationship [12].

To obtain γ_p it is necessary to find $(dC)/da$ which we have arranged to be independent of the crack length a, P the load at which the crack grows, and b the width of the crack.

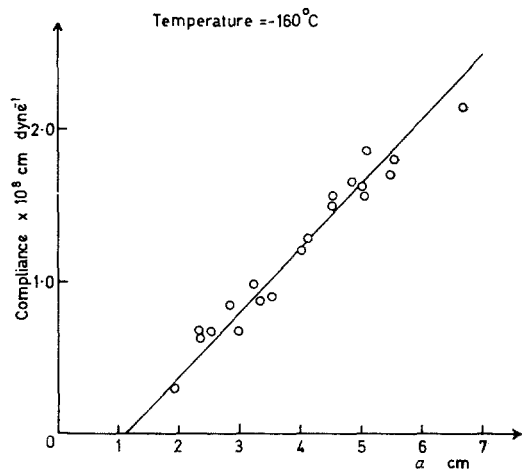

Figure 13 Compliance of amorphous cleavage specimens as a function of crack length.

TABLE II Variation of K for different crack lengths $W = 9.60$ cm.

	$a/W = 0.2$	$a/W = 0.3$	$a/W = 0.4$	$a/W = 0.5$	$a/W = 0.6$	$a/W = 0.7$
$KBW^{\frac{1}{2}}/P$	16.8	17.5	17.7	17.8	19.0	24.0

The compliance of amorphous specimens at − 160°C is plotted against crack length in fig. 13. This is a plot for a number of specimens of different molecular weights, and shows a linear relationship within experimental error for a between 2 and 6 cm. The scatter in the results is due to differences in the machined sizes of samples, friction in the clamps, and the difficulty in judging the position of the crack front. Stress relaxation was found not to be important even at 20°C. This was shown by loading the specimen in a few seconds to just below the load at which the crack grows, and then observing that the stress relaxation was smaller than 2% after an hour at constant strain.

Similar plots of compliance against crack length were obtained for crystalline specimens at − 160°C and for both amorphous and crystalline specimens at 20°C.

The results of $(dC)/da$ can be compared with Gross and Srawley's results assuming linear elastic behaviour, and that plane strain conditions are obtained at the crack tip.

We then have

$$\frac{dC}{da} = \frac{4b}{P^2}\gamma_p = \frac{2bK_c^2}{P^2E(1-\nu^2)}$$

i.e.

$$\frac{dC}{da} = \frac{2b}{E(1-\nu^2)\,WB^2}\left(\frac{K_cBW^{\frac{1}{2}}}{P}\right)^2 \quad (3.6)$$

Note that Gross and Srawley's results have been computed for ungrooved specimens, viz. $b = B$. Williams and co-workers [13] have used the expression bB instead of B^2 for grooved samples and this is assumed here.

The slight dependence of the stress-intensity factor on crack length predicted in table II is not detectable in the range of plots of compliance against crack length. Table III shows the values of $(dC)/da$ found, together with the values of the Young's Modulus obtained from equation 3.6 assuming a value of $\nu = 0.4$ [14].

These values are compared with the values obtained previously [14, 15], and are seen to be in reasonable agreement. The relationship, however, is not significantly altered if the conditions were plane stress instead of plane strain (See relationship 3.3.)

Results for the surface energies of the different

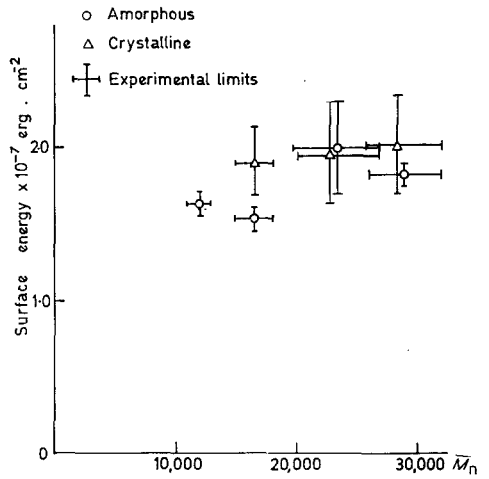

Figure 14 Variation of the surface energy for steady growth with molecular weight and crystallinity at − 160°C.

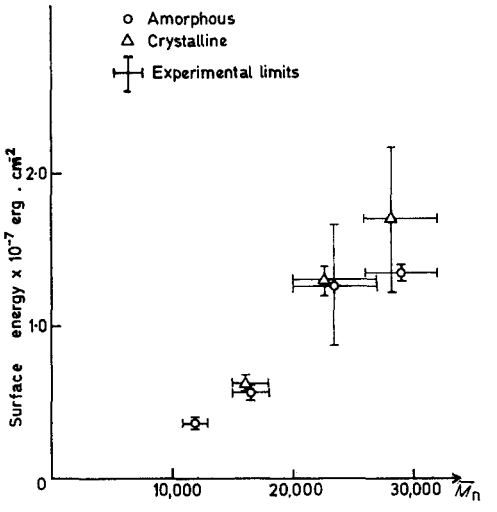

Figure 15 Variation of the surface energy for steady growth with molecular weight and crystallinity at 20°C.

TABLE III Experimental values of $(dC)/da$, calculated and observed values of Young's Modulus E.

	Temperature	$\frac{dC}{da}$ ($\times 10^8$ dynes^{-1})	E calculated ($\times 10^{-10}$ dynes/cm^{-2})	E observed [15] ($\times 10^{-10}$ dynes/cm^{-2})
Amorphous PET	20°C	0.71 ± 0.04	2.4 ± 0.1	2.2 ± 0.1
	− 160°C	0.43 ± 0.02	4.7 ± 0.1	4.1 ± 0.1
Crystalline PET	20°C	0.68 ± 0.03	2.4 ± 0.1	2.5 ± 0.1
	− 160°C	0.43 ± 0.02	4.7 ± 0.1	4.5 ± 0.1

materials are plotted in fig. 14 for − 160°C and in fig. 15 for 20°C. The surface energy values are all for controlled crack growth. The crack speed is in the range 1 to 0.01 cm/sec and can be deduced from the energy balance equation

$$\dot{a} = \frac{\dot{\delta}}{P(\mathrm{d}C)/\mathrm{d}a} \qquad (3.7)$$

where δ is the cross-head speed of the tensile testing machine.

At room temperature the crack speed could be measured by observing the movement of the crack past the lines of a grid marked on the specimen. The values thus obtained agree well with those calculated from the imposed cross-head speed. At − 160°C, only the calculated value of crack speed could be found.

The effect of crack speed in the range of 1 to 0.01 cm/sec cannot be observed within the scatter of several samples. However, if the cross-head speed is increased by a decade while a crack is growing, an increase in surface energy of the order 3% is observed. This result is obtained provided that the crack continues to grow in a stable manner. A more dramatic effect is that the more brittle materials cannot sustain fast cracks (speeds greater than $\simeq$ 1 cm/min) without causing uncontrolled rupture of the specimen by a number of cracks some of which deviate out of the side grooves. This result indicates that fast crack growth is possible at a much lower energy than 10^7 ergs/cm^2, but under unstable conditions.

It was found impossible to propagate cracks in the low-molecular-weight crystalline material in a controlled manner. The cracks jumped in a slip and stick manner as observed by Berry [16] for low-molecular-weight polymethylmethacrylate (PMMA). In such circumstances, it is possible to define two quantities, γ initiation and γ arrest [17] corresponding to the surface energies required at the onset of crack growth respectively.

The values obtained for low-molecular-weight crystalline material at 20°C are given below

$$\gamma \text{ initiation} = 5.0 \times 10^5 \text{ erg/cm}^{-2}$$
$$\gamma \text{ arrest} = 1.5 \times 10^5 \text{ erg/cm}^{-2}$$

The main features of the surface energy for controlled crack growth shown in figs. 14 and 15 can be summarised as follows:

(1) At − 160°C there is very little variation of the surface energy with molecular weight, the value of the surface energy being of the order 2×10^7 erg/cm^{-2}

(2) At 20°C there is a smooth change in surface energy with molecular weight the value changing from 2×10^7 erg/cm^{-2} for high-molecular-weight material to 0.3×10^7 erg/cm^{-2} for low-molecular-weight material.

(3) Crystalline materials have consistently higher values of surface energy than amorphous materials at both temperatures and for all molecular weights.

3.3.2. Surface features

The main features of all the steady growth fractures at − 160°C are the smooth regions and lines from the central part which is rough and drawn out. Fig. 16 shows these features, and in particular how the central region arises. The crack front is V-shaped and grows from the two side grooves into the centre. The V shown in the optical micrograph, fig. 16c, shows where the crack has been interrupted leaving a mark of where it was on the surface. The central drawn region shown in the scanning electron micrograph, figs. 16a and b, is seen to be the intersection of these two fronts. It appears that crazes grow in from the side grooves and then separate leaving interrupted smooth surfaces.

The important conclusion is that the crack front does not grow along the direction in which a is measured. This raises the question as to why the craze grows more readily from this side groove than from the end of the crack. In PMMA it is believed [8] that the crack propagates through a craze growing in the direction of the crack. We can therefore conclude that the machining of the surface of the groove encouraged crazing. In fact, specimens with grooves cut with a 90° milling cutter gave identical results. However, specimens grooved with the 0.015 cm saw blade from one side only did not, and in this case crazes initiated from the grooved side only. The cracks in such specimens did not grow in a stable manner but bifurcated after short crack growth.

Tests were also carried out on commercial grade PMMA specimens machined in the same manner as polyethylene terephthalate specimens. Slow propagation was obtained and the value of surface energy was:

$$\gamma_p = 2.2 \pm 0.1 \times 10^5 \text{ erg cm}^{-2}$$

at 20°C at a crack speed of 0.01 cm sec^{-1}. This value is comparable with that obtained by other workers [6, 7, 18] and the surface is smooth with the visible colours observed previously by Berry [19].

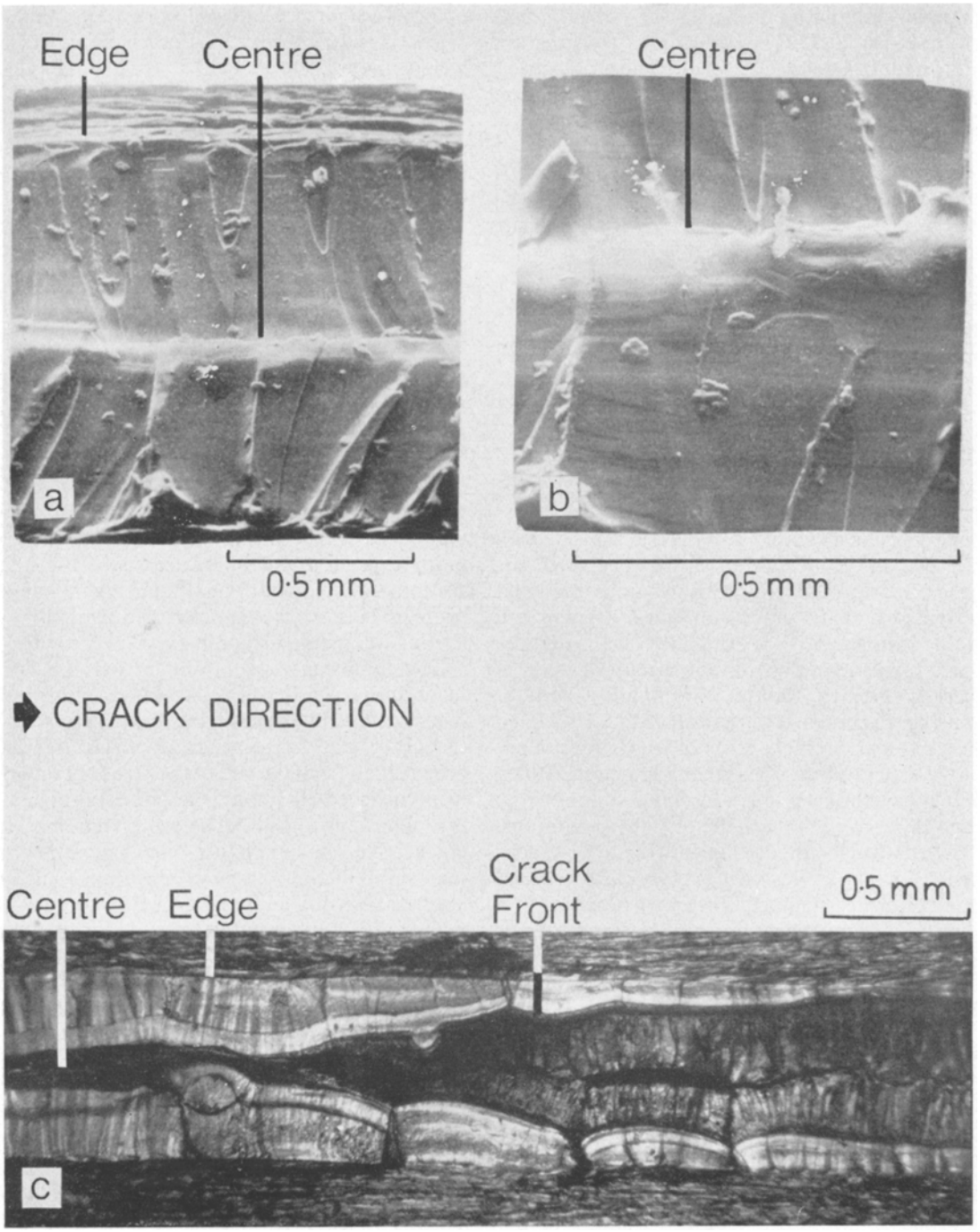

Figure 16 Cleavage surfaces for amorphous PET ($\bar{M}_n = 23\,000$) at − 160° C.

The next important feature of the low temperature cleavage surfaces is that flaws are visible as parabolic markings. These results are similar to those found in PMMA [19, 20], at fast crack speeds where it has been proposed that the flaw starts to open up before the crack front has reached it. The parabolic marking is thus the locus of the intersection of the planar crack front and the circular one. The same interpretation can be applied to our results. In this case, how-

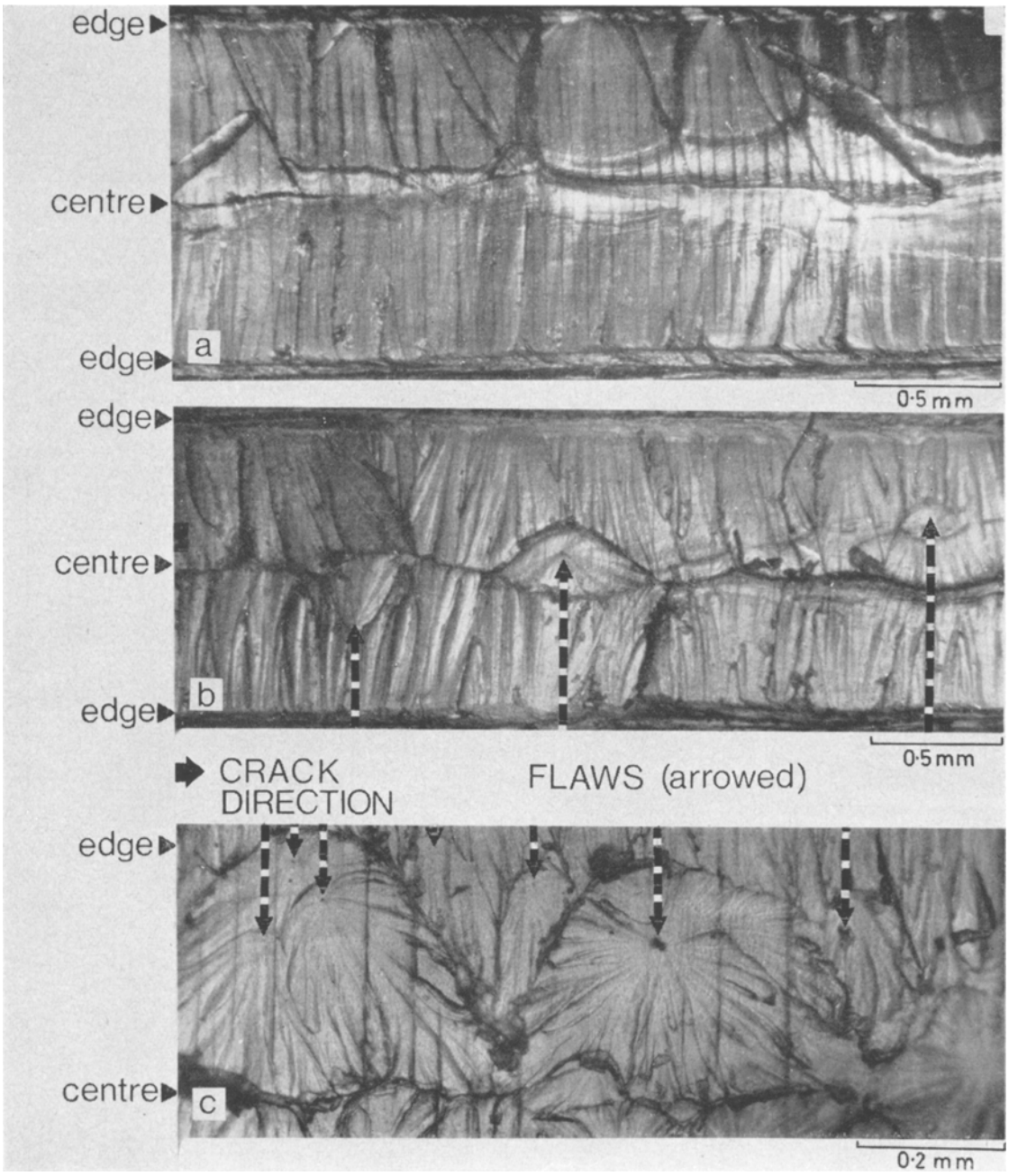

Figure 17 Cleavage surfaces for amorphous PET (a) $\overline{M}_n = 23000$. (b) $\overline{M}_n = 17000$. (c) $\overline{M}_n = 12000$ at $-160°C$.

ever, the axis of symmetry for the parabola is directed towards the central line as this is the direction in which the crack is growing.

These flaws are not visible on high-molecular-weight amorphous material. A few are found on medium-molecular-weight amorphous material and a number on the low-molecular-weight amorphous material. All the crystalline specimens show flaws. Fig. 17 is an optical micrograph of the cleavage surfaces, *a*, *b* and *c* being high-, medium- and low-molecular-weight amorphous material respectively. Fig. 18*a* is an optical micrograph and fig. 18b is an electron micrograph of the cleavage surfaces of a high-

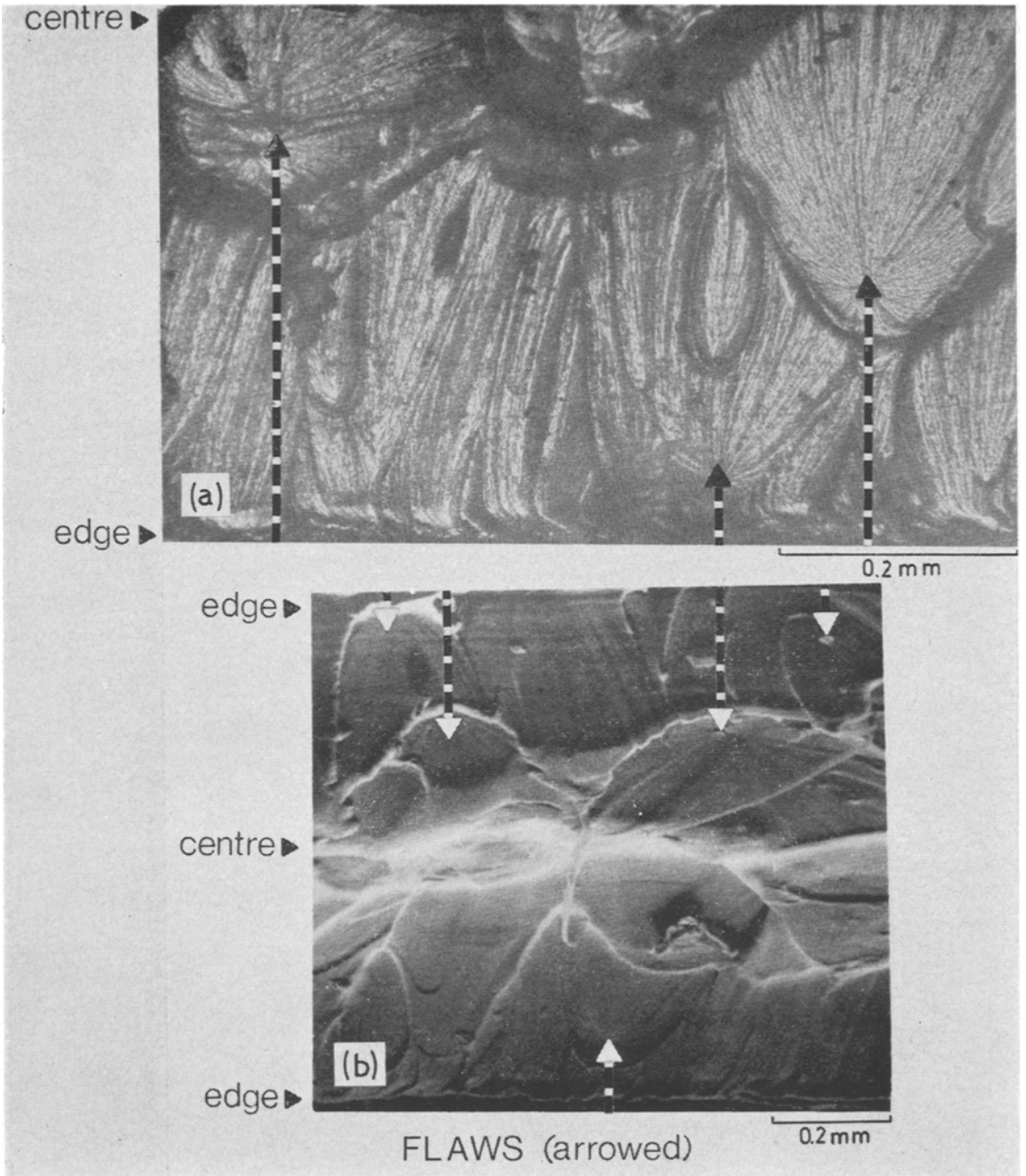

Figure 18 Cleavage surfaces for crystalline PET ($\bar{M}_n = 29\,000$) at $-160°$ C.

molecular-weight crystalline sample.

The third feature of these complex surfaces are the straight lines in the thickness direction, which can only be seen with transmitted light and are not observed in reflected light or in the electron microscope photographs. Viewing through the thickness direction these lines are seen to be crazes growing into the bulk of the specimen to a depth of about 0.02 cm. Because of the distribution of these crazes, i.e. a very few of them go through the central drawing region, it is suggested that they form at just about the time that the two crack fronts join to produce the central region.

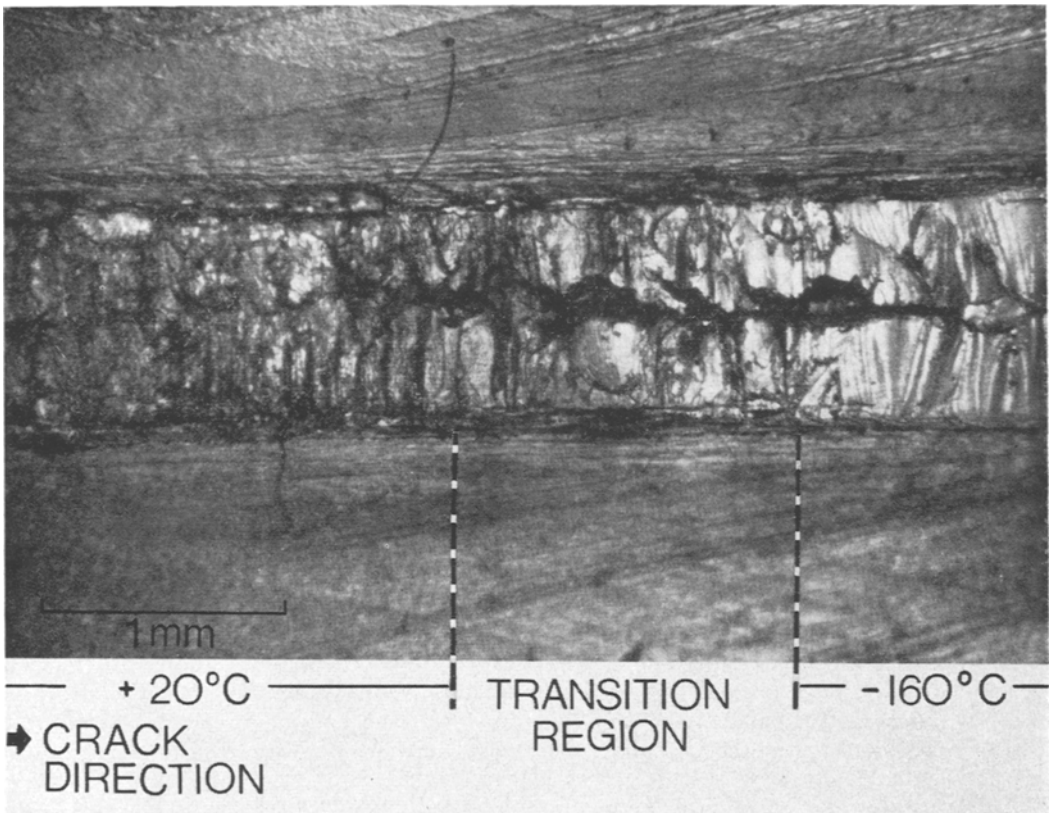

Figure 19 Cleavage surfaces for amorphous PET ($\bar{M}_n = 23000$) at 20 and − 160°C.

The fracture surfaces produced at 20°C are very rough and drawn out. Fig. 19 shows the transition from failure at 20°C to that at − 160°C. No differences are observed between the materials in spite of a five-fold change in surface energy. The crack front is not clearly defined and during a test the deforming region is of the order of 4 mm along the grooved section. Cracks are also visible growing into the bulk of the material to a depth of about 0.02 cm. The faster the crack is growing, the closer these cracks grow towards the direction in which the main crack is growing. This effect seems to correlate with the speed at which bifurcation takes place.

3.3.3. Failure mechanisms

At − 160°C the large surface energies observed are due to the nature of failure from crazes which grow not singly but in bulk before crack growth occurs.

The small increases of surface energy with crack speed can be attributed to the increase in yield stress for faster strain rates. It is possible to obtain much lower surface energies of the order of 10^5 erg cm^{-2} when the material fails in an uncontrolled manner from flaws.

These tests substantiate the suggestions put forward in section 3.1, namely that the high-molecular-weight material has less severe flaws than the low-molecular-weight amorphous material, and that crystallisation introduces flaws.

Because of the complexity of the crack growth in cleavage we cannot relate our results directly to those for tensile failure. The surface energy for cleavage at − 160°C is of the order 2×10^7 erg cm^{-2} where failure is from craze growth, compared to 5×10^5 erg cm^{-2} for tensile failures from a flaw. However, the results suggest that the differences between results for the different molecular weight specimens at − 160°C is due mainly to flaws. Crystalline specimens have slightly higher surface energies than amorphous specimens, consistent with their higher values of yield stress. The lower strengths of the crystalline specimens on the other hand, result from the

presence of larger flaws.

In discussing the results obtained at 20° C it is important to make one point clear. Failure of the high- and medium-molecular-weight material is only possible because of the side grooves which enable the drawing to be localised and not spread over the bulk of the specimen. This relates to what is observed with the notched tensile tests at 20° C.

Thus the cleavage test carried out here is really a miniature tensile test at the crack tip, and we are measuring the energy for rupture [21]. We shall now attempt to explain our results using this model assuming that the crack tip is the same for all the samples and the size of our miniature specimens are the same.

3.3.4. Comparison of cleavage and miniature tensile test at 20° C

3.3.4.1. Simple model

The simplest model was to measure the energy to rupture a dumbell sample in uniaxial tension. Samples with the dimensions shown in fig. 6a were extended to failure at a constant cross head speed of say S cm/sec. The energy to rupture the specimen was calculated from the area under the curve.

The best estimate for the length of the miniature sample is the width of the side groove, that is 0.015 cm. Although fine cracks travel into the bulk of the material to a depth of approximately 0.02 cm on either side, there is very little plastic work done in this region. For this reason it is not possible to see any differences between the fractured surfaces of the low- and high-molecular-weight amorphous materials, using a polarising microscope. The plastic work is thus confined within the side grooves.

Thus the energy per unit area to rupture a specimen of length 0.015 cm can be compared with the surface energy. It is necessary to do this at the appropriate strain rate. For the uniaxial tensile test the strain rate is estimated to be (S)/0.5 sec^{-1} which uses the observation that the length of the two necks is of the order 0.5 cm. For the cleavage test two assumptions are made to obtain the strain rate. Firstly it is observed that at 20° C material 0.4 cm distant from the crack tip is deforming. It is assumed therefore that the strain increases linearly from zero at a point 0.4 cm from the crack tip to a finite value at the crack tip. Secondly it is assumed that the strain at the crack tip is of the order of 2. This means that the material draws out to the same extent on the large dumbell samples. In this way the strain rate for a crack of velocity â cm/sec is $(\hat{a})/0.4 \times 2 = 5\hat{a}\ sec^{-1}$.

The comparison of this simple model with the surface energies is shown in table IV. The results show that the surface energies are of the same order as the work required to cold draw the material. This demonstrates the ductile nature of the behaviour. The model does not, however, explain the observed variation with molecular weight. Neither does the transition from cold drawing to necking rupture agree with the rate at which unstable cleavage fracture occurs.

3.3.4.2. Constrained tensile test

The simple model described above does not represent the material at the crack tip because of the contraints applied by the crack and the side grooves. It is essential to have side grooves in the cleavage specimens, otherwise the drawing will not be sufficiently localised for the test to be possible.

The cleavage results have therefore been compared with the work to rupture a constrained element and are shown in table V. The test involved extending a specimen 0.35 cm square and of length 2 cm. Around the central cross-section, saw cuts 0.015 cm wide were made

TABLE IV Comparison of cleavage and tensile tests for amorphous samples at 20° C.

	$\bar{M}_n = 12000$		$\bar{M}_n = 23000$		$\bar{M}_n = 29000$	
$\dot{e}$ sec^{-1}	Surface energy ($\times 10^{-7}$ erg cm^{-2})	Tensile energy ($\times 10^{-7}$ erg cm^{-2})	Surface energy ($\times 10^{-7}$ erg cm^{-2})	Tensile energy ($\times 10^{-7}$ erg cm^{-2})	Surface energy ($\times 10^{-7}$ erg cm^{-2})	Tensile energy ($\times 10^{-7}$ erg cm^{-2})
0.2 to 2	Not stable	0.05 (a)	1.3	0.1 to 1.0 (a)	1.4	0.1 to 1.0 (a)
0.02 to 0.2	0.4	0.05 (a)	1.3	2.6 b)	1.4	2.1 (b)
0.002 to 0.02	0.4	0.1 to 1.0 (a)	1.3	2.6 (a)	1.4	2.1 (b)
0.0002 to 0.00002		3.0 (b)				

(a) Denotes necking rupture. (b) Denotes cold drawing.

TABLE V Comparison of cleavage and constrained tensile tests at 20° C. $\dot{e} \simeq 0.002$ sec^{-1}.

$\bar{M}_n$	Amorphous		Crystalline	
	Surface energy ($\times 10^{-7}$ erg cm^{-2})	Constrained tensile energy ($\times 10^{-7}$ erg cm^{-2})	Surface energy ($\times 10^{-7}$ erg cm^{-2})	Constrained tensile energy ($\times 10^{-7}$ erg cm^{-2})
29000	1.4	1.3	1.7	1.1
23000	1.3	1.3	1.3	1.1
16000	0.6	0.9	0.6	—
12000	0.4	0.4	Not stable	—

TABLE VI Comparison of cleavage and notched impact tests [22] at 20° C.

$\bar{M}_n$	Amorphous		Crystalline	
	Surface energy ($\times 10^{-7}$ erg cm^{-2})	Impact strength (kgm cm/cm^2)	Surface energy ($\times 10^{-7}$ erg cm^{-2})	Impact strength (kgm cm/cm^2)
29000	1.4	3.5	1.7	2.7
23000	1.3	3.0	1.3	2.0
16000	0.6	2.6	0.6	1.7
12000	0.4	2.5	Not stable	—

on all four faces leaving a reduced cross-sectional area of 0.15 cm. The distance between the clamps was 0.5 cm and they were extended at a constant speed of 0.0001 cm sec^{-1}. The time to rupture was of the order of 1000 sec. The strain rate was calculated assuming that a strain of the order of 2 was obtained and was thus 0.002 sec^{-1}.

The results as shown in table V are in much better agreement than those of the simpler unconstrained model, table IV. The variation with molecular weight is now obtained in both tests. However, the differences between amorphous and crystalline materials are still not explained.

We can conclude that the room temperature cleavage data can be broadly explained in terms of very ductile deformation in a constrained region around the crack tip. The test thus not only involves strain hardening the material as in the simple model, section 3.3.4.1, but also voiding in front of the crack tip. These voids can be seen to open up in front of the crack tip during the cleavage tests. It is suggested that the fine cracks which are observed in the bulk of the material grow from these voids. Thus the behaviour is not only governed by strain hardening but by flaws. These are more important in the constrained tests because the constraints inhibit thinning of the crack width. Thus if the plastic strain is large voids must grow. It is further suggested that these voids grow from the flaws which cause brittle failure at − 160°C.

3.3.4.3. Comparison of cleavage fracture surface energy with impact strength

Table VI shows a comparison between notched impact strengths and cleavage fracture surface energies at 20°C. The impact strengths were observed on the same range of PET samples by Turner [22]. There is an equivalence between these two quantities. The cleavage test at 20°C, as explained, involves a large amount of plastic work in the constrained region near the crack tip. The notched impact strength involves the work required to initiate a fast crack from the notch. There exists reasonable correlation between the surface energy and the impact strength for the different molecular weight amorphous samples, indicating that both tests involve similar physical properties, strain hardening and inherent flaws. There is a difference, however, in comparing amorphous and crystalline samples in table VI. The surface energies for both amorphous and crystalline are similar, whereas the impact strength for the crystalline samples is lower than for the amorphous samples. This suggests that the effect of strain hardening and flaws in the two tests are not indentical. In particular, large flaws as observed previously in the crystalline material and the low-molecular-weight amorphous material, give comparatively lower impact strength. This is because impact involves initiation and hence is easier in those materials with large flaws. This is not reflected in the surface energies because these involve slow growth.

However, materials with low impact strength, or large flaws, will not deform in a stable manner at fast cleavage rates because of initiation of fast fracture from flaws.

4. Conclusions

(1) The tensile tests indicate that there are two processes initiating brittle failure in PET at − 160°C. The medium- and high-molecular-weight amorphous materials fail from crazes growing from the surface. In the low-molecular-weight amorphous material ($\bar{M}_n \simeq 12000$), and in all molecular weights of crystalline PET, failure is initiated by inherent flaws. The latter process may still be governed by craze growth but from an internal flaw rather than from a surface flaw. This conclusion is consistent with recent studies of yield and fracture of polymers under applied hydrostatic pressure [23]. Comparison of coated and uncoated specimens showed clearly that fracture in PMMA initiates at surface flaws, whereas fracture in crystalline PET initiates at internal flaws.

It has not in general been possible to obtain sharp cracks in the notched tensile and cleavage tests to ensure that single-crack propagation occurs. Because of this, very large cleavage fracture surface energies up to 2×10^7 erg cm^{-2} have been measured. However, the cleavage results at − 160°C clearly show the inherent flaws in those materials in which flaws were observed in tensile tests. Also there is a slight variation of surface energy with molecular weight, to form and break crazes, the low molecular weight being associated with a lower surface energy. This effect is still clearly shown in crystalline samples although these have higher surface energies than their amorphous counterparts which is consistent with their higher yield stress.

Two possible explanations can be proposed for the nature of the inherent flaws in these materials. These are that the flaws are crystalline amorphous boundaries or that they are associated with a number of chain ends acting together to form a defect in the amorphous region. We propose that the latter process predominates in the case of PET, and have two reasons for this.

Firstly, there is the similarity of the brittle strengths of the amorphous and crystalline low-molecular-weight materials at − 160°C, where the surface energies were found to be almost independent of crystallinity and molecular weight. We can conclude that the inherent flaw size is very similar in both cases. Secondly, the effect of molecular weight in all the tests is similar for amorphous and crystalline samples except when crazing intervenes as mechanism from which failure can arise. This indicates that the effect of chain ends is an overriding parameter in fracture. It is suggested that crystallinity does effect fracture behaviour by virtue of exclusion of chain ends from the crystalline regions. The amorphous material in a partially crystalline specimen therefore has a greater local concentration of chain ends than a wholly amorphous specimen of identical molecular weight. In other words, a partially crystalline specimen behaves similarly to an amorphous specimen of lower molecular weight.

(2) At 20°C the cleavage test is even more like a rupture test and the results correlate well with the energy to rupture tensile specimen at 20°C. Moreover, the change of surface energy with molecular weight is very similar to the variation of impact strength. The changes with crystallisation are however not similar for impact and cleavage tests. It is suggested that this is because crystallisation introduces flaws which are effective in reducing the notch root radius in the impact tests but have less effect on the cleavage tests, which are carried out sufficiently slowly to allow controlled rupture.

Acknowledgements

This research was carried out during the tenure of a Science Research Council CAPS studentship by J. S. Foot. We are indebted to ICI Ltd, Petrochemical and Polymer Laboratory as the industrial sponsor, and wish to thank our colleagues in the Laboratory for their advice and assistance.

References

1. J. M. STEARNE and I. M. WARD, *J. Mater. Sci.* **4** (1969) 1088.
2. A. VAN DER BOOGART and C. E. TURNER, *Trans. & J. Plastics Inst.* **31** (1963) 109.
3. Special ASTM Bulletin Report on Fracture Testing of high strength sheet material 29 (January 1960).
4. M. J. MANJOINE, Biaxial Brittle Fracture Tests. Paper No. 64-Met-3, *ASME* (May, 1964).
5. J. E. SRAWLEY and B. GROSS, NASA Report E-3701 (1967).
6. J. P. BERRY, *J. Appl. Phys.* **34** (1963) 62.
7. L. J. BROUTMAN and F. J. MCGARRY, *J. Appl. Polymer Sci.* **9** (1965) 589.
8. R. P. KAMBOUR and R. W. KOPP, *J. Polymer Sci.* A2 **7** (1969) 183.

9. E. H. YOFFE, *Phil. Mag.* **42** (1951) 739.
10. G. R. IRWIN, *Eng. Fracture Mech.* **1** (1968) 241.
11. J. P. BERRY, *ibid* **A1** (1963) 993.
12. G. R. IRWIN and J. A. KIES, *Welding J. Res. Suppl.* **33** (1954) 1935.
13. G. R. MARSHALL, L. E. CULVER, and J. G. WILLIAMS, *Plastics and Polymers* J. Plastics Inst. **36** (1968) p. 75.
14. P. R. PINNOCK, I. M. WARD, and J. M. WOLF, *Proc. Roy. Soc.* **A291** (1966) 267.
15. M. TAKAYANAGI, *Mem. Fac. Eng. Kyushu Univ.* **23** No. 1 (1963) 1.
16. J. P. BERRY, *J. Polymer Sci.* **A2** (1964) 4069.
17. R. GRIFFITH and D. G. HOLLOWAY, *J. Mater. Sci.* **5** (1970) 302.
18. J. J. BENBOW and F. C. ROESLER, *Proc. Phys. Soc.* **B 70** (1957) 201.
19. J. P. BERRY, *Nature* **185** (1960) 91.
20. S. B. NEWMAN and I. J. WOLOCK, *J. Appl. Phys.* **29** (1958) 49.
21. A. G. THOMAS, *J. Polymer Sci.* **18** (1955) 177.
22. R. M. TURNER, *Chem. and Ind.* (1970) 120.
23. S. RABINOWITZ, I. M. WARD, and J. S. C. PARRY, *J. Mater. Sci.* **5** (1970) 29.

Received 14 September and accepted 7 October 1971.